JCTC Journal of Chemical Theory and Computation

Article

pubs.acs.org/JCTC

Protonation of DMPC in a Bilayer Environment Using a Linear Response Approximation

Vitor H. Teixeira,[†] Diogo Vila-Viçosa,[†] António M. Baptista,[‡] and Miguel Machuqueiro*[,†]

[†]Centro de Química e Bioquímica, Departamento de Química e Bioquímica, Faculdade de Ciências, Universidade de Lisboa, 1749-016 Lisboa, Portugal

[‡]Instituto de Tecnologia Química e Biológica, Universidade Nova de Lisboa, Av. da República, 2780-157 Oeiras, Portugal

Supporting Information

ABSTRACT: pH is a very important property, influencing all important biomolecules such as proteins, nucleic acids, and lipids. The effect of pH on proteins has been the subject of many computational works in recent years. However, the same has not been done for lipids, especially in their most biologically relevant environment: the bilayer. A reason for this is the inherent technical difficulty in dealing with this type of periodic systems. Here, we tackle this problem by developing a Poisson−Boltzmann-based method that takes in consideration the periodic boundary conditions of lipid bilayer patches. We used this approach with a linear response approximation to calculate the pK_a value of a DMPC molecule when diluted in zwitterionic lipids. Our results show that DMPC protonation only becomes relevant at quite low pH values (2−3). However, when it happens, it has a strong impact on lipid conformations, leading to significant heterogeneity in the membrane.

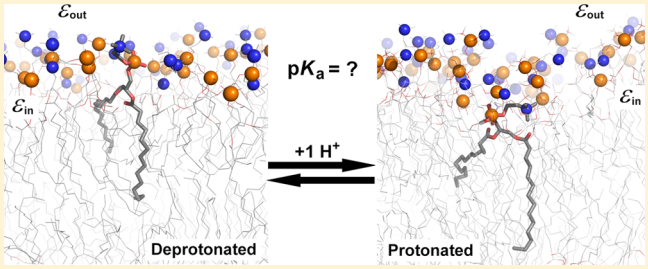

1. INTRODUCTION

Solution pH is a fundamental physicochemical property that directly influences the structure and function of various types of biological molecules.[1−6] Because of several difficulties inherent to these systems, it was only recently that an increasing number of works started to appear in the literature. Lipid protonation leads to changes in the electrostatic environment, which will affect the lipid bilayer, directly or indirectly interfering in many membrane-mediated biological processes such as membrane fusion, domain formation, drug−liposome interactions, and membrane phase transitions.[7−11] The mitochondrial membrane plays a crucial role in ATP synthesis (respiratory chain), which is dependent on the pH gradient across the membrane together with the membrane potential.[12−15]

The interpretation of the pH effect on a lipid bilayer and on its electrostatic environment is a challenging task. Theoretical methods can be very useful to understand this problem at a molecular level. With the constant evolution of computer power and algorithms, larger and more complex model systems have been treated using molecular modeling methods. Simulations with membrane systems are only now being fully explored, because of the extra complexity comparatively to protein systems. The first studies on membrane electrostatics used a simplified theory, which assumes that the charges on phospholipids are uniformly spread over a planar surface and that the solvent is a structureless medium with a uniform dielectric constant (Gouy−Chapman theory).[16] This simple theory was successfully used to explain the ζ-potential of phospholipid vesicles,[17] or how ions affect the surface potential above the phospholipid monolayers.[18] It was also shown that, for charged and well-organized membranes, the Gouy−Chapman theory is in good agreement with a more-detailed system representation with Poisson−Boltzmann (PB) theory.[19,20] Other works have analyzed the electrostatic interaction of proteins with charged flat surfaces[21] or discretized charged surfaces,[22] using the linearized form of the PB equation, to evaluate the best orientation and distance of interaction. Membrane interactions with peptides were also studied using lysine as a model with a mixture of anionic and zwitterionic phospholipids to access the binding free-energy dependence on the number of lysine residues, the salt concentration and percentage of acidic phospholipids.[20] From PB calculations, using several snapshots from molecular dynamics (MD) simulations, it was also possible to analyze the potential roughness near the membrane surface.[23]

The first attempt to calculate a pK_a shift in a membrane-like environment used a monolayer of docosyl amines treated with two-dimensional periodic boundary conditions (2D-PBC) in an air/water interface,[24] with the electrostatic potential obtained from the nonlinear PB equation. More recently, the lipid titration problem has also been addressed in micellar systems.[25−28] A mix of Monte Carlo (MC) and PB techniques were used trying to determine the pK_a shift of lauric acid in a neutral[25] and ionic micellar environment;[25,26] in ref 25, MC calculations are done in a discrete system that defines a radius for the hydrophobic region and includes the "lipid head groups" in the solvent region to be given a high dielectric constant.

Received: January 6, 2014
Published: April 4, 2014

   dx.doi.org/10.1021/ct5000082 | J. Chem. Theory Comput. 2014, 10, 2176−2184

Recently, a constant-pH MD methodology[29] was applied to study the pK_a of lauric acid under different conditions,[27,28] namely in micellar and membrane-like supramolecular assemblies. In all of these systems, the solutes were always completely solvated; therefore, the PBC were not taken into account[25−28] in the electrostatic calculations.

The objective of this work is to present a PB-based method to estimate the electrostatic potential in an infinite bilayer environment with atomic detail and use it for pK_a calculations. It borrows the theoretical/computational aspects associated with the thermodynamic cycle used in protein pK_a calculations, but requires several additional features inherent to the two-dimensional periodicity of membrane systems. PB calculations were performed on conformations from molecular dynamics (MD) simulations of a patch of phospholipids of finite dimensions. The inclusion of 2D-PBC in the electrostatic potential calculation in the membrane patches allows for an unprecedented realism in PB-based methods used in pK_a calculations of phospholipids. This new method was applied to the known zwitterionic phospholipid 1,2-dimyristoyl-*sn*-glycero-3-phosphocholine (DMPC). This is a well-parametrized system for which there is considerable structural information at the lamellar phase[30−43] and solid parameters for most biomolecular force fields.[44] The pK_a of the phosphate group in a DMPC bilayer is not known, but it its usually assumed to be very low, as the deprotonated (charged) form is usually used in MD simulations. We used a linear response approximation (LRA)[45,46] to calculate the pK_a value of one DMPC diluted in other zwitterionic DMPC molecules, thus providing an estimate of the pH where protonation of this lipid becomes relevant.

2. METHODS

2.1. Theoretical Considerations. One standard approach to determine the pK_a of protonatable groups is to calculate electrostatic properties using the PB equation, followed by a calculation of the probability of each protonation state along a pH range.[47−49] The PB equation can be solved through several methods such as finite differences, boundary element, and finite element. In the finite difference method,[50] as implemented in many programs, the potential is iteratively calculated in each grid point until the potential value converges. In this iterative process, an initial guess is made for the electrostatic potential at each grid point. The electrostatic potential at the boundaries of the grid does not change, keeping the first initial guess (Dirichlet boundary conditions). The described procedure works well for a localized system, such as a protein in solution (with approximate spherical symmetry), but that represents a problem when dealing with "infinite" systems like biological membranes (with approximate cylindrical symmetry), since the usual methods to estimate the initial potential (Coulombic, dipolar, etc.) are inadequate to take into account the virtually infinite membrane dielectric medium. A simple way to circumvent this problem is to use periodic boundary conditions along the directions parallel to the membrane (2D-PBC). The use of this approach in the calculation of the electrostatic potential allow us to determine pK_a values of phospholipids embedded in bilayers.

Even though DelPhi[51,52] is able to compute the electrostatic potential using periodicity, no such option exists for the surface calculation. When applied to a periodic MD configuration of the bilayer, this produces an irregular molecular shape near the walls of the finite difference grid, reflecting the way the system happened to be split across the walls of the MD simulation box. When this nonperiodic shape is used to assign the dielectric constant over the grid, two types of problems arise in the bilayer regions near the walls (see an illustration in Supporting Information). The first problem occurs when a grid point that should be in the low-dielectric region is assigned to the solvent region, because the nearby atomic sphere that would enclose it in the periodic case happens to be located on the opposite side of the grid in the nonperiodic case. The second problem is related to the fact that, in the radius assignment method adopted here (section 2.4), some hydrogen atoms are assigned a zero radius while remaining enclosed in the sphere of their non-hydrogen partner (this follows from their Lennard-Jones parameters in the GROMOS 54A7 force field); when such a hydrogen atom is near a wall, the nonperiodic treatment may place it and its partner on opposite sides of the grid, leaving the hydrogen not enclosed in any sphere and assigning its charge to the solvent region. In order to solve these problems, we added a small portion (5% of the box side dimension) of the system atoms in both *x*- and *y*-directions along which 2D-PBC are used (see the Supporting Information), with the added atoms being assigned their usual radius but a zero atomic charge. This procedure ensures the continuity of the bilayer molecular surface at the box walls and avoids placing charges in the solvent.

Another problem is when a titrating group falls on the boundary, split across the box, with atoms appearing on the other side of the box through 2D-PBC. This situation presents difficulties in the application of the focusing procedure, where a second finer and smaller box is used to calculate the electrostatic potential without 2D-PBC. One of the limitations is that the smaller box must be confined inside the larger and coarser one, impairing its application to a residue at the box edge. One simple way of preventing this problem, is to create an equivalent configuration in which the titrating group is centered on the grid. With this x/y centering procedure, the atomic charges will always be in the center of the grid.

Usually proteins can simply be inserted inside a box large enough to enclose it and to properly estimate the electrostatic terms needed to the pK_a calculation. However, in a membrane system, there is 2D-PBC and we should not calculate interactions with groups that are farther than half the x/y grid vector dimension. This problem can be circumvented by calculating pairwise and background interactions only within a given cutoff (see the Supporting Information).

Despite the above-mentioned procedures, the calculation of pK_a values in phospholipids embedded in a membrane is similar to the calculation in proteins. The methodology used here for the pK_a calculation is similar to the one previously published.[47] To calculate the pK_a value of a phosphate group of a DMPC molecule, we can use eq 1:

$$\mathrm{p}K_i = \mathrm{p}K_i^{\mathrm{int}} + \sum_{j \neq i} W_{ij} \tag{1}$$

where the first term is the intrinsic pK_a and the second term corresponds to the direct interactions between different titrating groups of the system. pK^{int} is the pK when all other titrable groups are fixed in a reference state, which, in our case, is the charged state[48] and can be written as

$$\mathrm{p}K^{\mathrm{int}} = \mathrm{p}K^{\mathrm{mod}} - \gamma \frac{(\Delta\Delta G_{\mathrm{Solv}} + \Delta\Delta G_{\mathrm{Back}})}{2.3 k_{\mathrm{B}} T} \tag{2}$$

where pK^{mod} is the pK of the model compound; $\gamma = 1$ or -1, depending on the group being cationic or anionic, respectively; G_{Solv} is the solvation free-energy difference; G_{Back} is the background contribution difference; k_B is the Boltzmann constant; and T is the absolute temperature. The solvation free energy of transferring a molecule between two different dielectric media can be obtained directly from the output of the DelPhi[51,52] program, using the induced charge method (see ref 51 for details). The background contribution is the interaction energy from nontitrating partial charges and can be computed as

$$\Delta\Delta G_{Back} = \sum_i q_i[\phi^C_{memb}(r_i) - \phi^N_{memb}(r_i)] - \sum_i q_i[\phi^C_{model}(r_i) - \phi^N_{model}(r_i)] \quad (3)$$

where q_i are the nontitrating partial charges located at r_i, and the superscripts C and N denote charged and neutral states, respectively. The second term in eq 3, relative to the model compound, is zero.

The last term in eq 1 corresponds to the direct interactions between pairs of titrating groups of the system and is calculated as

$$W_{ij} = w_{ij}(1, 1) - w_{ij}(1, 0) - w_{ij}(0, 1) + w_{ij}(0, 0) \quad (4)$$

where $w_{ij}(n_i,n_j)$ is the electrostatic interaction energy between sites i and j. The four terms in eq 4 correspond to the possible combinations of the protonation states of a pair of sites and, 1 and 0 stands for protonated or deprotonated, respectively. As an example, the second term in eq 4 gives the electrostatic interaction energy when site i is protonated and site j is deprotonated and can be calculated as

$$w_{ij}(1, 0) = \frac{1}{2}\sum_i (Q_i^C \phi_i^{jN}) + \frac{1}{2}\sum_j (Q_j^N \phi_j^{iC}) \quad (5)$$

where the first sum runs over all atoms of site i and the second over all atoms of site j. Q_x^y is the nth charge of site x in the protonation state y and $\phi_x^{z^y}$ is the electrostatic potential on site x when site z is in protonation state y.

2.2. Parameterization of DMPC Molecule. There are atomic partial charges for DMPC in the literature,[53] but only for the zwitterionic form where the phosphate group is deprotonated. Since our objective is to do pK_a calculations of DMPC, we need atomic partial charges of this phospholipid in both protonated and deprotonated forms. We determined a new set of atomic partial charges following a procedure similar to that previously used for the zwitterionic form.[53] DMPC molecule geometry was optimized with Gaussian 03[54] at the HF/6-31G(d) level, and the resulting electrostatic potential was fitted to atomic coordinates with RESP[55] with P and N fixed to the Mulliken charges. The final atomic charges were slightly adjusted to be consistent with the charge groups of the GROMOS96 54A7 force field and are given as Supporting Information.

2.3. MM/MD. Molecular mechanics/dynamics simulations were performed with GROMACS version 4.0.7.[56,57] The GROMOS 54A7 force field[58,59] was used, which already includes the DMPC corrections,[44] together with the atomic partial charges determined in this work. All MD simulations started from an equilibrated lipid bilayer with 128 DMPC molecules and 4038 SPC water molecules,[60] totaling 18 770 atoms per system. An orthorhombic simulation box was used, applying periodic boundary conditions in all three directions and the minimum image convention, as usual when using an explicit solvent. The x/y and z box vectors varied around 62 and 69 Å, respectively, ensuring that the membrane does not see its periodic image along the z-direction. The simulations were done in the NPT ensemble, using Berendsen heat baths[61] at 310 K with separate couplings for the solute and solvent with a relaxation time of 0.1 ps, while a Berendsen semi-isotropic pressure couple[61] was used to keep the pressure at 1 bar with isothermal compressibility of 4.5×10^{-5} bar^{-1} and a relaxation time of 2.0 ps. All lipid bond lengths were constrained using the parallel version of the LINCS algorithm,[62] and the SETTLE algorithm[63] was used for water. The equations of motion were integrated using a time step of 2 fs. Nonbonded interactions were treated with a twin-range method, using group-based cutoffs of 8 and 14 Å, updated every 5 steps (10 ps). Long-range electrostatics thus truncated were corrected with a reaction field, using a dielectric constant of 54.0.[64] No ions were added to the systems.

A three-step energy minimization was performed consisting of a steepest-descent calculation followed by another using the low-memory Broyden–Fletcher–Goldfarb–Shanno algorithm without constraints nor restraints. A final minimization with steepest-descent using constraints in all bonds was performed.

Initialization of the molecular dynamics runs occurred in 2 steps. First, a 50-ps MD simulation was done with all heavy atoms position-restrained with a force constant of 1000 kJ/(mol nm^2). Initial velocities were taken from a Maxwellian distribution at 310 K. In the second step, a 200-ps MD simulation was done with position restraints in all phosphorus (P) atoms using a force constant of 1000 kJ/(mol nm^2).

Table 1 shows the list of production runs performed. System Sys1 presents all 128 lipid molecules in the deprotonated zwitterionic form, while systems Sys2a–e have two DMPC molecules protonated, one in each monolayer. The 10 protonated phospholipids were selected randomly. For analysis, these 10 phospholipids were also chosen in Sys1, although we could have taken any of the 128 lipids, since they are all equivalent.

Table 1. MD Simulations Performed with DMPC Bilayers with the Random Selected Phospholipids in Each Monolayer

system	state	lipid 1[a]	lipid 2[a]
Sys1	Deprot		
Sys2a	Prot	54	65
Sys2b	Prot	4	119
Sys2c	Prot	16	99
Sys2d	Prot	24	75
Sys2e	Prot	50	51

[a]Lipid 1 and 2 are located in different monolayers. The numbers refer to the topological lipid residue number in the simulations.

All simulations started from the same pre-equilibrated simulation and were run for 500 ns each. Calculations and analysis were performed in the last 450 ns equilibrated segments of each system (Table 1), with conformations saved every 10 ps.

2.4. Poisson–Boltzmann/Monte Carlo. The Poisson–Boltzmann (PB) calculations were done with the program DelPhi V5.1,[51,52] using radii taken from the GROMOS 54A7 force field[58,59] and partial charges derived in this work (see

above). The molecular surface of the membrane was defined by a probe of radius 1.4 Å, the ion exclusion layer was 2.0 Å, and the ionic strength was 0.1 M. The dielectric constant of the solvent was 80, and for the membrane, we used values of 2, 4, 6, and 8 (see results and refs 46, 65−67 for a discussion of these values). In the coarse grid, we used relaxation parameters of 0.2 and 0.75 to help both the linear and nonlinear iteration convergence processes. Considering the membrane oriented along the *xy* plane, we explicitly applied PBC in the calculation of the potential in both the *x*- and *y*-directions in the coarse grid (2D-PBC).

A cutoff of 25 Å (see results) was used to calculate the background interactions. The convergence threshold value based on maximum change of potential was set to 0.01. The PB calculations were done in a cubic grid with 61 grid points and a two-step focusing,[68] where the focus grid was one-fourth of the coarser grid size. The conformations were taken from the MD simulations preformed in NPT. Since the dimension of the box changes along the simulation, the space between grid points for the coarser grid must be calculated for every conformation (average values of ∼1.0 and ∼0.25 Å for the coarse and focus grids, respectively). The Monte Carlo (MC) sampling was performed with the PETIT program.[48] All runs were performed using 10^5 MC cycles, where one cycle consists of sequential state changes over all individual sites.

Conformations for PB/MC calculations were taken from the six MD simulations (Table 1) from the equilibrated last 450 ns of each system at intervals of 10 ps. This makes 45 000 frames per system in a total of 270 000 frames. Since the titrating groups (Table 1) are to far away from each other, they do not interact and are not included in the pairwise interaction calculations. This way, the groups can be treated independently with increased sampling.

2.5. Linear Response Approximation. The linear response approximation (LRA) has been successfully used to determine pK_a values of amino acid residues in proteins.[45,46] This method was used here to compute the pK_a value of a phosphate group in a DMPC molecule embedded in a lipid bilayer, and can be calculated using the expression

$$\mathrm{p}K_a = \frac{1}{2}[\langle \mathrm{p}K_a(c)\rangle_p + \langle \mathrm{p}K_a(c)\rangle_d] \quad (6)$$

where p$K_a(c)$ is the pK_a when the system is fixed in conformation *c*, and the angled brackets denote averages over the conformations sampled from the MD simulations with the site protonated (p) or deprotonated (d). The pK_a value for each conformation, p$K_a(c)$, was obtained from MC runs at different pH values using the PB-derived free-energy terms (see sections 2.1 and 2.4).

The reorganization energy[46,69,70] is the free energy needed to change the protonated system to configurations typical of the deprotonated state (and vice versa), and can be calculated using the expression

$$\lambda = \frac{1}{2}[\langle \mathrm{p}K_a(c)\rangle_p - \langle \mathrm{p}K_a(c)\rangle_d] \quad (7)$$

2.6. Analysis. Several tools from the GROMACS software package[56,57] were used, and others were developed in-house. The individual areas per lipid headgroup were calculated using the GridMAT-MD tool.[71] The calculations of correlation-corrected errors for averages were computed using standard methods based on the autocorrelation function of the property measured to determine the number of independent blocks in the simulations.[72]

3. RESULTS AND DISCUSSION

3.1. Effect of Protonation on Membrane Structural Features. We evaluated several structural properties of our bilayers and compared them with the available experimental data. The area per lipid (A_l) is probably the most important property to access the system equilibration and to determine the correct liquid state of a lipid bilayer. Figure 1 shows the A_l of all simulations over time. This property is difficult to measure experimentally and significantly different values can be obtained from different approaches and methodologies.[30−43] Our Sys1 result shows an A_l value in the lower limit, but still within the experimental range (Figure 1). This slightly lower A_l value is the result of a small difference between our charge set and the one from Chiu and co-workers.[53] The A_l value of the deprotonated system is slightly higher than the values observed for the protonated ones. The presence of a proton decreases the electrostatic repulsion in the neighbor phosphate groups, stabilizing them through hydrogen bonds. To characterize the environment around the protonated lipid, we envisaged a radial descriptor where we divide the membrane plane in concentric circles (of radii *r*) centered on a specific phospholipid in a way that each annulus has a width *w*, and *r* goes from ∼3.5 Å to 20 Å in steps of ∼0.5 Å (Figure 2a). Figure 2b illustrates the decrease in the A_l value of the zwitterionic DMPC lipids as they approach the protonated one. The A_l value for this protonated lipid (45.4 Å^2) is remarkably low, typical from a gel phase. Thus, protonation of a DMPC molecule induces a local contraction of the membrane.

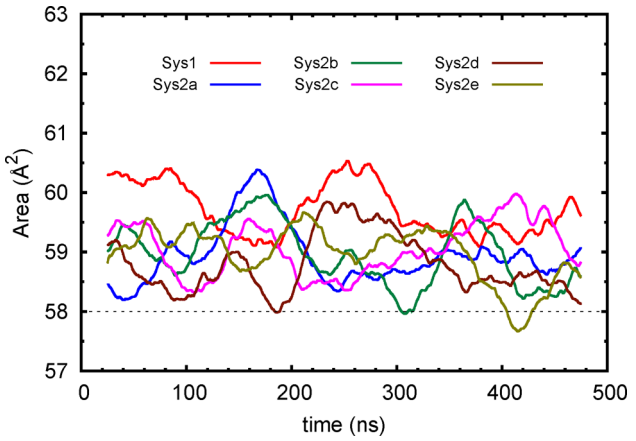

Figure 1. A_l values of all simulations over time. System Sys1 is pure zwitterionic DMPC, while in systems Sys2a−e, there are two protonated DMPC molecules. The dashed line defines the lower limit of the experimental range (∼58 Å^2) with the upper limit (∼65 Å) being outside of the plot *y*-range.[30−43] A floating window average (50 ns) was applied for clarity.

The diffusion coefficient can be obtained from the Einstein relation by measuring the slope of the mean square deviation (MSD) over time from the linear part of the curve.[72] We obtained the values 6.2 × 10^{-8} and 7.6 × 10^{-8} cm^2/s for the deprotonated and protonated, respectively (Figure 3). These values are within the experimental range ((5−10) × 10^{-8} cm^2/s).[73] The small increase in the diffusion coefficient for the protonated DMPC was not expected and indicates some

dx.doi.org/10.1021/ct5000082 | J. Chem. Theory Comput. 2014, 10, 2176−2184

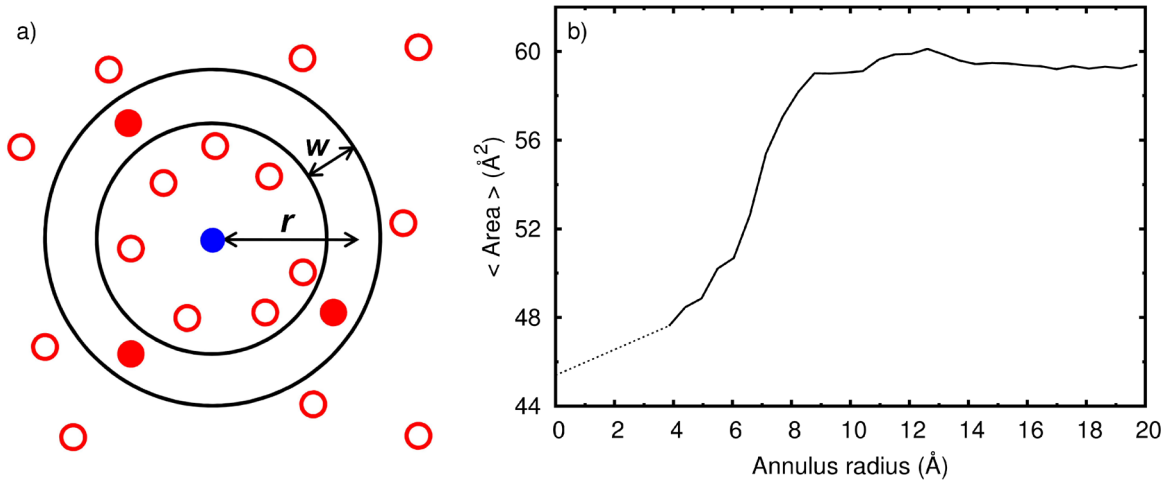

Figure 2. Radial A_l description around the lipid of interest: (a) graphic representation of the sliding annulus with $r - w/2$ as the smaller radius and $r + w/2$ as the larger radius; (b) average A_l value along a sliding annulus of 0.5 Å width. At the zero radius, we plotted the average A_l for the protonated DMPC. The individual areas of each lipid were calculated with the GridMAT-MD tool.[71]

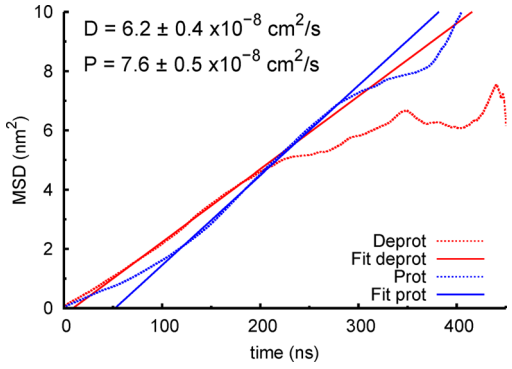

Figure 3. MSD, over time, for protonated (blue) and deprotonated (red) DMPC in a membrane. The deprotonated was fitted between 50 and 200 ns, while the protonated one was fitted between 100 ns and 300 ns.

instability factor that is able to overcome the hydrogen bond network formed.

Figure 4 shows the order parameter profiles for the protonated and deprotonated forms. Both systems show order parameters a little above the experimental values (Figure 4), still all have $|S_{CD}|$ values lower than 0.25, indicating that the aliphatic chains are disordered.[33] The fact that protonation induces minor disorder to the system while still lowering its A_l prompted us to look at the protonated phosphate groups in detail.

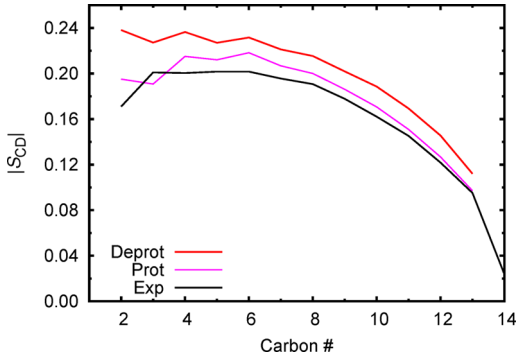

Figure 4. Deuterium order parameters averaged over sn-1 and sn-2 chains of DMPC, compared with experimental values interpolated to 310 K.[42]

3.2. Phosphate Distribution along the Membrane Normal. The phospholipids in membranes are not static, and, although we did not observe flip−flop events, they move considerably. These movements are observed not only in the membrane plane, but also in the membrane normal. Looking at a specific phospholipid, we can follow the z-position of its P atom, relative to the other 63 in the same monolayer (P_r) (Figure 5a). These P_r values oscillate over a large range (~15 Å) for both protonation states (Figure 5b). The histograms of P_r distribution illustrate a clear difference for the protonated species, namely, its insertion into the membrane. While the deprotonated phospholipids are distributed around the overall zero position, upon protonation, the distribution moves toward the inside of the membrane ~3 Å. The neutralization of the phosphate group in DMPC may be favoring both the desolvation (moving away from the solvent) and the interactions with the ester groups deeper in the membrane. In addition, the choline positive group can now push, with less resistance, the lipid toward the membrane in order to interact directly with the neighboring negatively charged phosphates.

3.3. Phosphate Protonation Induces a Local Depression. The previous analysis showed that protonation induced a significant insertion of the lipid in the bilayer. In order to characterize the possible membrane deformation, we calculated P_r as we did in the previous section, but using, as reference only, the phospholipids that fall inside a sliding annulus (red filled circles in Figure 2a). The resulting profile (Figure 6) shows how the average z-positions of the other phosphate groups in the DMPC bilayer (P_r^*) changes with distance. Similar to what was observed previously (Figure 5b), the P_r^* values of the deprotonated system expectedly fluctuate around the position of the lipid of interest. The protonated system added some structural detail regarding the organization of its neighbors. As we increase the annulus radius, P_r^* increases up to a distance of ~6−7 Å, where it stabilizes (note that the P_r^* values were adjusted so that zero was assigned to the z-position of the lipid of interest). At this distance, P_r^* is ~2.5 Å and increased to 3.0 Å at higher radius. A similar result has been observed with lauric acid, where its solvent-accessible surface

dx.doi.org/10.1021/ct5000082 | J. Chem. Theory Comput. 2014, 10, 2176−2184

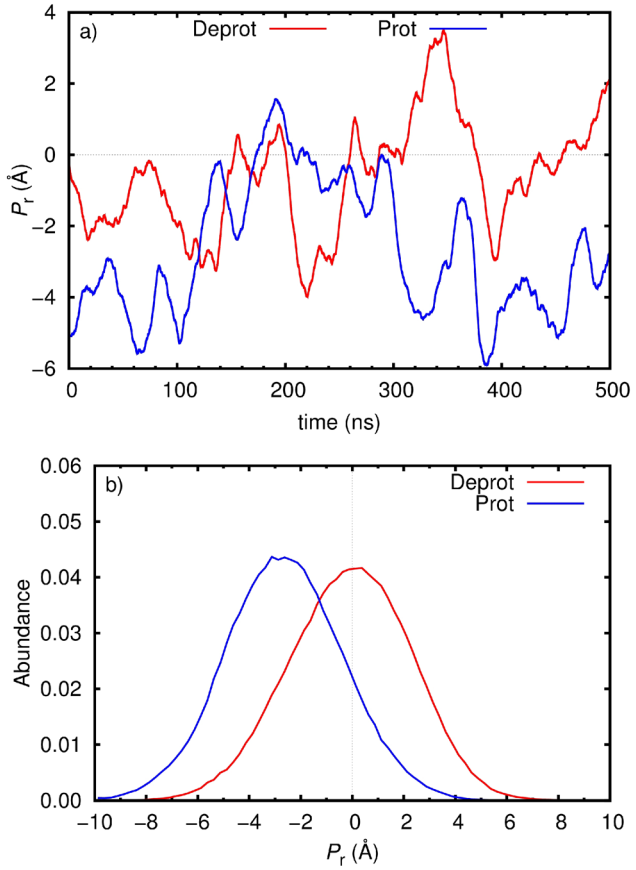

Figure 5. P_r distribution relative to the membrane normal: (a) floating window average (20 ns) of P_r over time for one specific lipid (lipid 65) in both protonation states; (b) the P_r distribution histograms for all lipids studied.

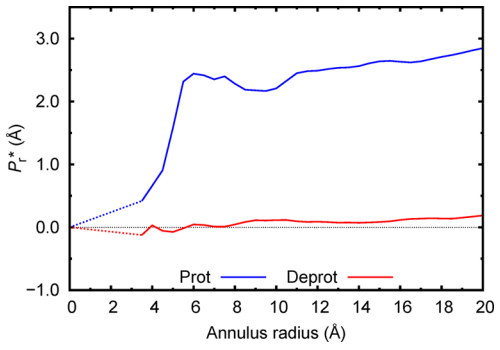

Figure 6. Radial depth description around the lipid of interest. P_r^* values are relative to the sliding annulus. The P_r^* values were adjusted so that the zero was assigned to the lipid of interest.

decreased upon protonation.[27] The bell-shaped depression in the DMPC bilayer that occurs upon protonation of one lipid (Figure 6) is also characterized by internalized deprotonated lipids situated in the first interacting sphere. These lipids seem to be dragged into a deeper region of the bilayer by the protonated DMPC. This is probably only possible because the protonated lipid becomes a hydrogen bond donor in a large excess of hydrogen bond acceptors, and it is able to network with multiple neighbors. The impact of protonation in the interaction of our lipid of interest and its neighbors was already hinted by the average specific area of the protonated DMPC (Figure 2b), and it can also be illustrated using a radial distribution function (rdf).

The rdf analysis was done over all phospholipids of interest (Table 1) using only their P position. Figure 7 shows that the

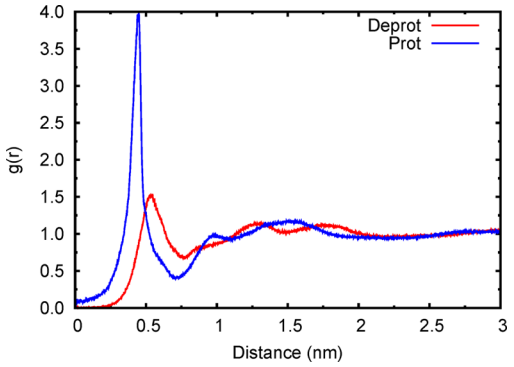

Figure 7. Average 2D-radial distribution of deprotonated phospholipids around the lipid of interest. Only the phosphor atoms were used in the calculations.

protonated DMPC molecule interacts more strongly with its neighbors than the deprotonated form. The hydrogen bonding and the absence of the negative charge can contribute to a significant decrease in the distance peak observed for the first shell of interacting lipids. This result is in accordance with the low A_l value of protonated DMPC (45.4 Å^2), and it helps to explain the smaller A_l value observed in Sys2, relative to Sys1, although, because of the existence of only one protonated phospholipid per monolayer, this difference is not significant in the final A_l value of Figure 1.

3.4. pK_a Calculation Using a Linear Response Approximation. The pK_a of the phosphate group of DMPC embedded in a bilayer is not known, although the first pK_a of phosphate in water is 2.12.[74] In DMPC, the phosphate group is doubly functionalized being similar to the dimethyl phosphate whose pK_a in water is 1.29,[75] which was used as the pK^{mod} value. Here, we used the LRA method to compute the pK_a of one DMPC molecule in a pure bilayer of deprotonated DMPC. Even though this is not the midpoint pK_a value of a DMPC membrane, it corresponds to the pH at which DMPC starts to become protonated and exhibit heterogeneous behavior. The values computed at different dielectric constants are shown in Table 2. The interior dielectric constant (ε_{in}) in proteins has

Table 2. pK_a Values from LRA at Different Interior Dielectric Constants (ε_{in}); Reorganization Energies (λ) Are Also Presented

ε_{in}	pK_a (LRA)	λ (pK units)
2	5.5 (±1.2)	8.0
4	3.3 (±0.6)	4.3
6	2.6 (±0.4)	3.1
8	2.2 (±0.3)	2.4

been the subject of many discussions,[45,46,49,65] but values between 2 and 8 have been adopted within the LRA methodology.[46,65−67] Although a value of ε_{in} = 2 should work if both states have been well sampled *and* if their distributions extensively overlap, this is certainly not the case for the system under study: indeed, the large local change induced by protonation in the membrane structure (Figure 6) points to a

dx.doi.org/10.1021/ct5000082 | J. Chem. Theory Comput. 2014, 10, 2176−2184

poor overlap, corroborated by the significant reorganization energy obtained even at high ε_{in} values (Table 2). In such cases, the LRA method was found to require a larger ε_{in} value (6 or 8).[46,65] Therefore, from Table 2, we can estimate a pK_a value of ~2.2−2.6. It is important to note that this is only one estimate of the pH at which the first DMPC gets protonated in an infinite bilayer of deprotonated lipid. Nevertheless, these values support most theoretical MD simulations with pure DMPC, where authors usually ignore phosphate protonation.

We observed a considerable degree of structural deformation upon DMPC protonation, with the protonated lipid populating different regions along the membrane normal, comparing with its deprotonated counterpart. Figure 8 shows how that

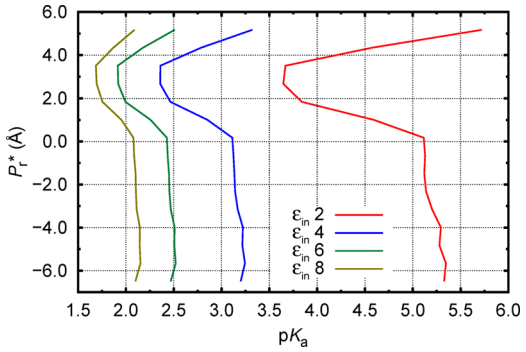

Figure 8. pK_a values at different P_r^* positions of the membrane normal. The bin size of the P_r^* has a fixed dimension of 0.833 Å.

heterogeneity affects the calculated pK_a values. Having the P_r^* and the pK_{half} values for the phospholipids of interest, we calculated the pK_a values using LRA in small portions along the membrane normal. The plot shows the pK_a profile along the membrane normal. The lowest pK_a was observed at 2−3 Å, which corresponds to an average position of the positive choline groups that can stabilize the negative (deprotonated) phosphate group, lowering its pK_a value. Going deeper into the membrane, the pK_a values increase as a result of unfavorable electrostatic interactions between the negatively charged phosphate groups. In addition, the protonated form can be stabilized through hydrogen bonds with neighbor phosphate groups and especially with the esters. The high pK_a values observed above 3 Å were obtained with a very limited number of protonated conformations, which results in poor sampling. These few conformations were special because they consisted in a protonated phosphate pairing through hydrogen bonding with a deprotonated neighbor, which resulted in significantly higher pK_a values.

4. CONCLUSIONS

We present here a new approach to calculate pK_a values in lipid bilayers using Poisson−Boltzmann theory, together with periodic boundary conditions. This allows the calculation of the electrostatic properties in different types of periodic systems, such as membranes.

The pK_a calculations were done using LRA with several dielectric constant values for the bilayer. Based on the substantial local rearrangement observed in the MD simulations, a moderately higher ε_{in} was selected (6−8). As a result, we estimate that relevant DMPC protonation will only happen at very low pH values (2−3). Therefore, our results support the decision of using zwitterionic DMPC in most theoretical MD simulation studies.

Some important structural properties such as A_l, diffusion coefficient, and order parameters were calculated and showed to be within the experimental ranges for liquid-crystalline Lα phase DMPC. The protonation of 1 DMPC molecule (in 64) did not affect the membrane properties significantly, probably because its effect became diluted. However, the protonation led to a decrease in the specific A_l value and to the internalization of the phosphate group, and formation of a local depression. This was favored by the hydrogen bond network that the protonated phosphate was able to do with other phosphates and esters. In addition, the neutral phosphate does not need to be solvated as much as the charged one. One of the consequences of the hydrogen bonding was the dragging of its closest neighbors, which resulted in a bell-shaped local depression.

The approach here presented can easily be generalized to other lipid bilayers. The inclusion of this method within the constant-pH MD framework[76−85] will certainly open new research opportunities to characterize, at the molecular level, systems where pH and phase transitions are strongly coupled. Furthermore, if, with pure PC systems, pH seems to play only a minor role, for lipid bilayers containing anionic lipids, this most probably will not be the case.

■ ASSOCIATED CONTENT

Supporting Information

Images with the atomic partial charges of DMPC in both protonated and deprotonated states. Procedure to determine the truncation cutoff for the electrostatic interactions. This material is available free of charge via the Internet at http://pubs.acs.org/.

■ AUTHOR INFORMATION

Corresponding Author

*Tel.: +351-21-7500112. Fax: +351-21-7500088. E-mail: machuque@fc.ul.pt.

Notes

The authors declare no competing financial interest.

■ ACKNOWLEDGMENTS

We thank Maria J. Calhorda, João Henriques, Paulo J. Costa, Sara R. R. Campos, and Hugo A. F. Santos for fruitful discussions. We acknowledge financial support from Fundação para a Ciência e a Tecnologia (through Project Nos. PTDC/QUI-BIQ/113721/2009 and PEst-OE/QUI/UI0612/2013 and Grant No. SFRH/BD/81017/2011).

■ REFERENCES

(1) Stryer, L. *Biochemistry*, 4th Edition; W. H. Freeman & Company: New York, 1995.
(2) Matthew, J. *Annu. Rev. Biophys. Biophys. Chem.* **1985**, *14*, 387−417.
(3) Honig, B. H.; Hubbell, W. L.; Flewelling, R. F. *Annu. Rev. Biophys. Biophys. Chem.* **1986**, *15*, 163−193.
(4) Sharp, K.; Honig, B. *Annu. Rev. Biophys. Biophys. Chem.* **1990**, *19*, 301−332.
(5) Warshel, A. *Annu. Rev. Biophys. Biophys. Chem.* **1991**, *20*, 267−298.
(6) Martel, P.; Baptista, A.; Petersen, S. *Biotechnol. Annu. Rev.* **1996**, *2*, 315−372.

(7) Chernomordik, L.; Leikina, E.; Frolov, V.; Bronk, P.; Zimmerberg, J. *J. Cell Biol.* **1997**, *136*, 81−93.
(8) Redfern, D.; Gericke, A. *J. Lipid Res.* **2005**, *46*, 504−515.
(9) Carrozzino, J.; Khaledi, M. *J. Chromatogr. A* **2005**, *1079*, 307−316.
(10) Cevc, G.; Watts, A.; Marsh, D. *Biochemistry* **1981**, *20*, 4955−4965.
(11) Zhou, Y.; Raphael, R. *Biophys. J.* **2007**, *92*, 2451−2462.
(12) Wang, J. H. *Annu. Rev. Biophys. Bioeng.* **1983**, *12*, 21−34.
(13) Deckers-Hebestreit, G.; Altendorf, K. *Annu. Rev. Microbiol.* **1996**, *50*, 791−824.
(14) Schultz, B.; Chan, S. *Annu. Rev. Biophys. Biomol. Struct.* **2001**, *30*, 23−65.
(15) von Ballmoos, C.; Wiedenmann, A.; Dimroth, P. *Annu. Rev. Biochem.* **2009**, *78*, 649−672.
(16) Bockris, J.; Reddy, A. *Modern Electrochemistry: An Introduction to an Interdisciplinary Area*; Plenum Press: New York, London, 1970.
(17) McLaughlin, S.; Harary, H. *Biochemistry* **1976**, *15*, 1941−1948.
(18) MacDonald, R.; Bangham, A. *J. Membr. Biol.* **1972**, *7*, 29−53.
(19) Peitzsch, R.; Eisenberg, M.; Sharp, K.; McLaughlin, S. *Biophys. J.* **1995**, *68*, 729−738.
(20) BenTal, N.; Honig, B.; Peitzsch, R.; Denisov, G.; McLaughlin, S. *Biophys. J.* **1996**, *71*, 561−575.
(21) Yoon, B.; Lenhoff, A. *J. Phys. Chem.* **1992**, *96*, 3130−3134.
(22) Roush, D.; Gill, D.; Willson, R. *Biophys. J.* **1994**, *66*, 1290−1300.
(23) Li, Z.; Venable, R.; Rogers, L.; Murray, D.; Pastor, R. *Biophys. J.* **2009**, *97*, 155−163.
(24) Smart, J.; McCammon, J. *J. Am. Chem. Soc.* **1996**, *118*, 2283−2284.
(25) da Silva, F.; Bogren, D.; Söderman, O.; Åkesson, T.; Jönsson, B. *J. Phys. Chem. B* **2002**, *106*, 3515−3522.
(26) Söderman, O.; Jönsson, B.; Olofsson, G. *J. Phys. Chem. B* **2006**, *110*, 3288−3293.
(27) Morrow, B.; Wang, Y.; Wallace, J.; Koenig, P.; Shen, J. *J. Phys. Chem. B* **2011**, *115*, 14980−14990.
(28) Morrow, B.; Koenig, P.; Shen, J. *J. Chem. Phys.* **2012**, *137*, 194902−194902.
(29) Lee, M.; Salsbury, F.; Brooks, C. *Proteins: Struct. Funct. Bioinf.* **2004**, *56*, 738−752.
(30) Nagle, J.; Tristram-Nagle, S. *Biochim. Biophys. Acta, Biomembr.* **2000**, *1469*, 159−195.
(31) Costigan, S.; Booth, P.; Templer, R. *Biochim. Biophys. Acta, Biomembr.* **2000**, *1468*, 41−54.
(32) Kučerka, N.; Liu, Y.; Chu, N.; Petrache, H.; Tristram-Nagle, S.; Nagle, J. *Biophys. J.* **2005**, *88*, 2626−2637.
(33) Petrache, H.; Dodd, S.; Brown, M. *Biophys. J.* **2000**, *79*, 3172.
(34) Rand, R.; Parsegian, V. *Biochem. Biophys. Acta* **1989**, *988*, 351−376.
(35) Smaby, J. M.; Momsen, M. M.; Brockman, H. L.; Brown, R. E. *Biophys. J.* **1997**, *73*, 1492−1505.
(36) Lewis, B. A.; Engelman, D. M. *J. Mol. Biol.* **1983**, *166*, 211−217.
(37) De Young, L. R.; Dill, K. A. *Biochemistry* **1988**, *27*, 5281−5289.
(38) Balgavỳ, P.; Dubničková, M.; Kučerka, N.; Kiselev, M. A.; Yaradaikin, S. P.; UhrÌĄková, D. *Biochim. Biophys. Acta, Biomembr.* **2001**, *1512*, 40−52.
(39) Lis, L.; McAlister, M.; Fuller, N.; Rand, R.; Parsegian, V. *Biophys. J.* **1982**, *37*, 657.
(40) Janiak, M.; Small, D.; Shipley, G. *J. Biol. Chem.* **1979**, *254*, 6068−6078.
(41) Koenig, B.; Strey, H.; Gawrisch, K. *Biophys. J.* **1997**, *73*, 1954−1966.
(42) Petrache, H.; Tristram-Nagle, S.; Nagle, J. *Chem. Phys. Lipids* **1998**, *95*, 83−94.
(43) Kučerka, N.; Kiselev, M. A.; Balgavý, P. *Eur. Biophys. J.* **2004**, *33*, 328−334.
(44) Poger, D.; Mark, A. E. *J. Chem. Theory Comput.* **2010**, *6*, 325−336.
(45) Lee, F. S.; Chu, Z. T.; Warshel, A. *J. Comput. Chem.* **1993**, *14*, 161−185.
(46) Eberini, I.; Baptista, A.; Gianazza, E.; Fraternali, F.; Beringhelli, T. *Proteins: Struct. Funct. Bioinf.* **2004**, *54*, 744−758.
(47) Baptista, A. M.; Martel, P. J.; Soares, C. M. *Biophys. J.* **1999**, *76*, 2978−2998.
(48) Baptista, A. M.; Soares, C. M. *J. Phys. Chem. B* **2001**, *105*, 293−309.
(49) Teixeira, V. H.; Cunha, C. C.; Machuqueiro, M.; Oliveira, A. S. F.; Victor, B. L.; Soares, C. M.; Baptista, A. M. *J. Phys. Chem. B* **2005**, *109*, 14691−14706.
(50) Klapper, I. *Proteins: Struct. Funct. Genet.* **1986**, *1*, 47−59.
(51) Rocchia, W.; Sridharan, S.; Nicholls, A.; Alexov, E.; Chiabrera, A.; Honig, B. *J. Comput. Chem.* **2002**, *23*, 128−137.
(52) Li, L.; Li, C.; Sarkar, S.; Zhang, J.; Witham, S.; Zhang, Z.; Wang, L.; Smith, N.; Petukh, M.; Alexov, E. *BMC Biophys.* **2012**, *5*, 9.
(53) Chiu, S.; Clark, M.; Balaji, V.; Subramaniam, S.; Scott, H.; Jakobsson, E. *Biophys. J.* **1995**, *69*, 1230−1245.
(54) Frisch, M. J.; Trucks, G. W.; Schlegel, H. B.; Scuseria, G. E.; Robb, M. A.; Cheeseman, J. R.; Montgomery, J. A., Jr.; Vreven, T.; Kudin, K. N.; Burant, J. C.; Millam, J. M.; Iyengar, S. S.; Tomasi, J.; Barone, V.; Mennucci, B. et al. *Gaussian 03, Revision C.02*; Gaussian, Inc.: Wallingford, CT, 2004.
(55) Bayly, C.; Cieplak, P.; Cornell, W.; Kollman, P. *J. Phys. Chem.* **1993**, *97*, 10269−10280.
(56) van der Spoel, D.; Lindahl, E.; Hess, B.; Groenhof, G.; Mark, A. E.; Berendsen, H. J. C. *J. Comput. Chem.* **2005**, *26*, 1701−1718.
(57) Hess, B.; Kutzner, C.; Van Der Spoel, D.; Lindahl, E. *J. Chem. Theory Comput.* **2008**, *4*, 435−447.
(58) Schmid, N.; Eichenberger, A.; Choutko, A.; Riniker, S.; Winger, M.; Mark, A.; Van Gunsteren, W. *Eur. Biophys. J.* **2011**, *40*, 843−856.
(59) Huang, W.; Lin, Z.; van Gunsteren, W. F. *J. Chem. Theory Comput.* **2011**, *7*, 1237−1243.
(60) Hermans, J.; Berendsen, H. J. C.; van Gunsteren, W. F.; Postma, J. P. M. *Biopolymers* **1984**, *23*, 1513−1518.
(61) Berendsen, H. J. C.; Postma, J. P. M.; van Gunsteren, W. F.; DiNola, A.; Haak, J. R. *J. Chem. Phys.* **1984**, *81*, 3684−3690.
(62) Hess, B. *J. Chem. Theory Comput.* **2008**, *4*, 116−122.
(63) Miyamoto, S.; Kollman, P. *J. Comput. Chem.* **1992**, *13*, 952−962.
(64) Smith, P.; van Gunsteren, W. *J. Chem. Phys.* **1994**, *100*, 3169−3174.
(65) Schutz, C. N.; Warshel, A. *Proteins: Struct. Funct. Genet.* **2001**, *44*, 400−417.
(66) Archontis, G.; Simonson, T. *Biophys. J.* **2005**, *88*, 3888−3904.
(67) Machuqueiro, M.; Campos, S. R.; Soares, C. M.; Baptista, A. M. *J. Phys. Chem. B* **2010**, *114*, 11659−11667.
(68) Gilson, M.; Sharp, K.; Honig, B. *J. Comput. Chem.* **1987**, *9*, 327−335.
(69) Marcus, R. A.; Sutin, N. *Biochem. Biophys. Acta* **1985**, *811*, 265−322.
(70) Churg, A. K.; Weiss, R. M.; Warshel, A.; Takano, T. *J. Phys. Chem.* **1983**, *87*, 1683−1694.
(71) Allen, W. J.; Lemkul, J. A.; Bevan, D. R. *J. Comput. Chem.* **2009**, *30*, 1952−1958.
(72) Allen, M.; Tildesley, D. *Computer Simulation of Liquids*; Oxford University Press: New York, 1987.
(73) Almeida, P. F. F.; Vaz, W. *Handbook of Biological Physics*, Vol. *1*; Elsevier: Amsterdam, 1995; pp 305−357.
(74) Bjerrum, J.; Schwarzenbach, G.; Sillen, L. G. *Stability Constants*, Special Publication No. 7; The Chemical Society: London, 1958.
(75) Kumler, W.; Eiler, J. *J. Am. Chem. Soc.* **1943**, *65*, 2355−2361.
(76) Baptista, A. M.; Teixeira, V. H.; Soares, C. M. *J. Chem. Phys.* **2002**, *117*, 4184−4200.
(77) Machuqueiro, M.; Baptista, A. M. *J. Phys. Chem. B* **2006**, *110*, 2927−2933.
(78) Machuqueiro, M.; Baptista, A. M. *Biophys. J.* **2007**, *92*, 1836−1845.
(79) Machuqueiro, M.; Baptista, A. M. *Proteins* **2008**, *72*, 289−298.
(80) Machuqueiro, M.; Baptista, A. M. *J. Am. Chem. Soc.* **2009**, *131*, 12586−12594.

(81) Machuqueiro, M.; Baptista, A. M. *Proteins: Struct. Funct. Bioinf.* **2011**, *79*, 3437−3447.
(82) Campos, S. R. R.; Machuqueiro, M.; Baptista, A. M. *J. Phys. Chem. B* **2010**, *114*, 12692−12700.
(83) Vila-Viçosa, D.; Campos, S. R. R.; Baptista, A. M.; Machuqueiro, M. *J. Phys. Chem. B* **2012**, *116*, 8812−8821.
(84) Henriques, J.; Costa, P. J.; Calhorda, M. J.; Machuqueiro, M. *J. Phys. Chem. B* **2013**, *117*, 70−82.
(85) Vila-Viçosa, D.; Teixeira, V. H.; Santos, H. A. F.; Machuqueiro, M. *J. Phys. Chem. B* **2013**, *117*, 7507−7517.

NOTE ADDED AFTER ASAP PUBLICATION

This article was published ASAP on April 21, 2014. Due to a production error, references 65−75 in the reference list were not in the correct order. The corrected version of the manuscript was published ASAP on May 1, 2014.